Forensic Sciences Research, 2023, **8**, 140–151
https://doi.org/10.1093/fsr/owad014
Advance access publication date 22 May 2023
Research Article

How to sample a seizure plant: the role of the visualization spatial distribution analysis of *Lophophora williamsii* as an example

Jiaman Lin[1,2,†], Keming Yun[1,†], Qiran Sun[2], Ping Xiang[2], Lina Wu[1,2], Shuo Yang[2], Junling Dun[3], Shanlin Fu[1], Hang Chen[2,*]

[1]School of Forensic Medicine, Shanxi Medical University, Key Laboratory of Forensic Medicine in Shanxi Province, Key Laboratory of Forensic Toxicology of Ministry of Public Security, Jinzhong, China
[2]Department of Forensic Toxicology, Shanghai Key Laboratory of Forensic Medicine, Academy of Forensic Science, Shanghai, China
[3]Shimadzu (China) Co., Ltd, Shanghai, China

*Corresponding author. E-mail: chenh@ssfjd.cn

[†]Jiaman Lin and Keming Yun are co-first authors.

Abstract

Natural compounds in plants are often unevenly distributed, and determining the best sampling locations to obtain the most representative results is technically challenging. Matrix-assisted laser desorption/ionization mass spectrometry imaging (MALDI-MSI) can provide the basis for formulating sampling guideline. For a succulent plant sample, ensuring the authenticity and *in situ* nature of the spatial distribution analysis results during MSI analysis also needs to be thoroughly considered. In this study, we developed a well-established and reliable MALDI-MSI method based on preservation methods, slice conditions, auxiliary matrices, and MALDI parameters to detect and visualize the spatial distribution of mescaline *in situ* in *Lophophora williamsii*. The MALDI-MSI results were validated using liquid chromatography–tandem mass spectrometry. Low-temperature storage at −80°C and drying of "bookmarks" were the appropriate storage methods for succulent plant samples and their flower samples, and cutting into 40 μm thick sections at −20°C using gelatin as the embedding medium is the appropriate sectioning method. The use of DCTB (trans-2-[3-(4-tert-butylphenyl)-2-methyl-2-propenylidene]malononitrile) as an auxiliary matrix and a laser intensity of 45 are favourable MALDI parameter conditions for mescaline analysis. The region of interest semi-quantitative analysis revealed that mescaline is concentrated in the epidermal tissues of *L. williamsii* as well as in the meristematic tissues of the crown. The study findings not only help to provide a basis for determining the best sampling locations for mescaline in *L. williamsii*, but they also provide a reference for the optimization of storage and preparation conditions for raw plant organs before MALDI detection.

Key Points

- An accurate *in situ* MSI method for fresh water-rich succulent plants was obtained based on multi-parameter comparative experiments.
- Spatial imaging analysis of mescaline in *Lophophora williamsii* was performed using the above method.
- Based on the above results and previous results, a sampling proposal for forensic medicine practice is tentatively proposed.

Keywords: forensic toxicology; sampling; spatial distribution; MALDI-MSI; peyote; *Lophophora williamsii*; mescaline

Introduction

Plant-based substances constitute a large group in seizure cases, according to the United Nations Office on Drugs and Crime reports [1, 2]. Narcotic plant or drug-related plant samples are one type of sample that may be involved in every forensic science laboratory. However, the sampling of live plant samples is sometimes a troublesome problem. It is often unrealistic to use the whole plant as an analytical sample because of the destructive nature of current mainstream drug analysis methods. The natural distribution of natural compounds in plants is often not uniform [3–5]. Unsupported random sampling may not yield representative results, resulting in a failure to achieve the objectives of forensic analysis.

Mass spectrometry imaging (MSI) is a technique that can realistically reflect the target compound's spatial distribution in the sample analysis [6, 7]. The MSI result may be a valid basis for the formulation of sampling and the basis for explaining the analysis results. MSI methods include matrix-assisted laser desorption/ionization (MALDI) imaging, secondary ion MSI, desorption electrospray ionization imaging, laser ablation electrospray ionization imaging, etc. [8–10]. Of these methods, MALDI-MSI is a well-established and easy-to-use ionization imaging method that is widely used in basic research [11, 12]. It has appropriate sensitivity that makes it suitable for many samples in forensic practice [13–16], but it also has a wide range of resolutions, making it useful for both fine-area (tens of microns) and wide-area imaging. In our previous study, the preliminary spatial distribution of mescaline in various cactus plants was obtained by MALDI-MSI, and the mechanism of mescaline production, transport, and storage was discussed in combination with the other studies [17].

Received: February 15, 2023. **Accepted:** May 16, 2023
© The Author(s) 2023. Published by OUP on behalf of the Academy of Forensic Science.
This is an Open Access article distributed under the terms of the Creative Commons Attribution Non-Commercial License (https://creativecommons.org/licenses/by-nc/4.0/), which permits non-commercial reuse, distribution, and reproduction in any medium, provided the original work is properly cited.
For commercial reuse, please contact journals.permissions@oup.com

More refined MSI results are affected by many parameters, such as the sample preservation method [18–20], slicing techniques [21, 22], sample preparation method [23–27], sample embedding/fixation method [28–30], auxiliary matrices [31, 32], and sampling ionization profile (laser diameter, ion beam, or surface contact area) [33]. In addition, for MALDI, the distribution of the sprayed matrix [34, 35] and participation of the biological sample's own matrix elements [36] are further influencing factors that cannot be ignored. For succulent plants, the above effects may be more noteworthy in the MSI analysis.

Lophophora williamsii (peyote) is a typical succulent member of the Cactaceae family [37], but it has received forensic attention because of its natural mescaline (β-3,4,5-trimethoxyphenethylamine) content. Mescaline is a compound with hallucinogenic activity in humans [38] and is listed as regulated in many countries [39–41]. As a natural component of this plant, its presence and content are affected by various culture conditions and the environment [42]. In forensics cases, seized plants may contain mescaline, but whether the content of mescaline exceeds the limit of local legal control is the question most frequently asked by forensic scientists. Knowledge of the distribution of mescaline in *L. williamsii* may therefore be helpful for developing a credible sampling and analysis guideline and may provide a more reasonable explanation of the analyzed results.

In the present study, we first developed a more refined, reliable MALDI-based MSI method based on preservation methods, slicing conditions, auxiliary matrices, and MALDI parameters. Next, we used this method to analyze the spatial distribution of mescaline in actual *L. williamsii* plants. Finally, based on the results of this analysis and our previous study, we have tentatively proposed a sampling suggestion.

Experimental

Chemicals and materials

Regents and materials

Mescaline and 25B-NBOMe-D_3 (IS) were purchased from Cerilliant (Round Rock, TX, USA). MALDI grade α-cyano-4-hydroxycinnamic acid (CHCA, 97.0%), 2,5-dihydroxybenzoic acid (DHB, 98.0%), Super-DHB (S-DHB, ≥98.0%), 9-aminoacridine (9-AA, ≥99.5%), 1,5-diaminonaphthalene (1,5-DAN, ≥99.0%), 2,5-dihydroxyacetophenone (2,5-DHAP, 97.0%), and dithranol (DT, ≥90%), as well as HPLC-grade methanol (MeOH) and acetonitrile (ACN), were purchased from Sigma-Aldrich (St. Louis, MO, USA). MALDI grade trans-2-[3-(4-tert-butylphenyl)-2-methyl-2-propenylidene] malononitrile (DCTB, >98.0%) was purchased from TCI (Shanghai) Development Co. Ltd (Shanghai, China). HPLC-grade formic acid (FA, 98%) was purchased from Fluka (Buchs, Switzerland). HPLC-grade trifluoroacetic acid (TFA), dichloromethane (DCM), and tetrahydrofuran (THF) were purchased from CNW, ANPEL Laboratory Technologies Inc (Shanghai, China). Difco™ Gelatin and Tissue-Tek Optimum Cutting Temperature Compound, which were used for embedding, were purchased from Becton, Dickinson, and Co. (Sparks, MD, USA) and Sakura Finetek Japan Co. (Tokyo, Japan), respectively. Indium tin oxide (ITO)-coated glass slides (dimensions 75 × 25 × 1 mm, sheet resistivity ≤5 Ω) and double-sided carbon conductive tape (dimensions 12 mm × 20 m, resistivity <5 Ω/mm^2), which were used for MALDI-MSI, were purchased from South China Science & Technology Co. Ltd (Shenzhen, China) and SPI supplies (West Chester, PA, USA), respectively. Ultrapurified water was prepared using a Milli-Q water purification system (Millipore Corp.; Burlington, MA, USA).

Solutions

A standard stock solution of mescaline (10 μg/mL) was prepared in MeOH and diluted to the desired concentrations before use. A working internal standard (IS) solution with a concentration of 10 ng/mL was prepared by dilution in methanol. Based on previous studies [33, 43], the matrix was selected to prepare 10 mg/mL of CHCA, DHB, S-DHB, 9-AA, 1,5-DAN, and 2,5-DHAP in ACN/water (50/50, v/v) with 0.1% TFA, and a 10 mg/mL solution of DT was prepared in THF. The matrix deposition on the sample sections was tested using a matrix solution of DCTB prepared by dissolving 15 mg of DCTB powder in 50 μL DCM and then adding 1.45 mL ACN.

Plants

Three plant samples were obtained from real forensic cases. A preliminary DNA verification had confirmed the characteristic DNA sequence of *L. williamsii*. Sample 1 and Sample 2 consisted only of the crown and stem, as the plant roots had partly rotted. The live *L. williamsii* samples were spineless cacti with a gray–green colour (Figure 1). Sample 1 was long and cylindrical, about 9.1 cm long and 1.9 cm wide (the above lengths do not include roots, and the width is the widest part of the plant); it had five ribs with four areoles on each rib. Sample 2 was long and cylindrical, about 6.2 cm long and 2.1 cm wide; it had five ribs with three areoles on each rib. Sample 3 was spherical, about 5.2 cm long and 2.9 cm wide; it had five ribs with three areoles on each rib. These areoles were spineless and hairy. The center of the crown of Sample 3 was a specialized flower-bearing area of the cactus and was densely woolly or hairy. Sample 3 bloomed several times after a period of cultivation. The Ethics Committee of the Academy of Forensic Science approved the use of the sample and the study.

Sample pretreatments

Sampling and preservation

The surfaces of the *L. williamsii* plants were gently washed with deionized water and allowed to dry naturally at room temperature. Samples 1 and 2 were cut in half along the longitudinal axis with a scalpel, and each plant half was used as a separate group (Figure 1). The other treatments are shown in Table 1. The petals and sepals of Sample 3 were carefully collected, flattened, sandwiched between two layers of airlaid paper (Kimberly-Clark Professional, Mumbai, Maharashtra, India), and pressed in a book to make a "bookmark", as MALDI analysis requires a flat sample surface. The flattened samples were then stored at room temperature for later use.

Sample preparation for MALDI-MSI analysis

Sectioning of the plant material

The *L. williamsii* sample in Group A was embedded in paraffin and cut into 8 μm thick slices with a microtome (Leica RM2135, Wetzlar, Germany). The sections were mounted on conventional glass slides and then dewaxed and dehydrated in xylene and ethanol, respectively. Limited by the lyophilization storage procedure, samples of Group B shrunk and could not be embedded or sliced. The *L. williamsii* samples in Groups C and D were submerged in

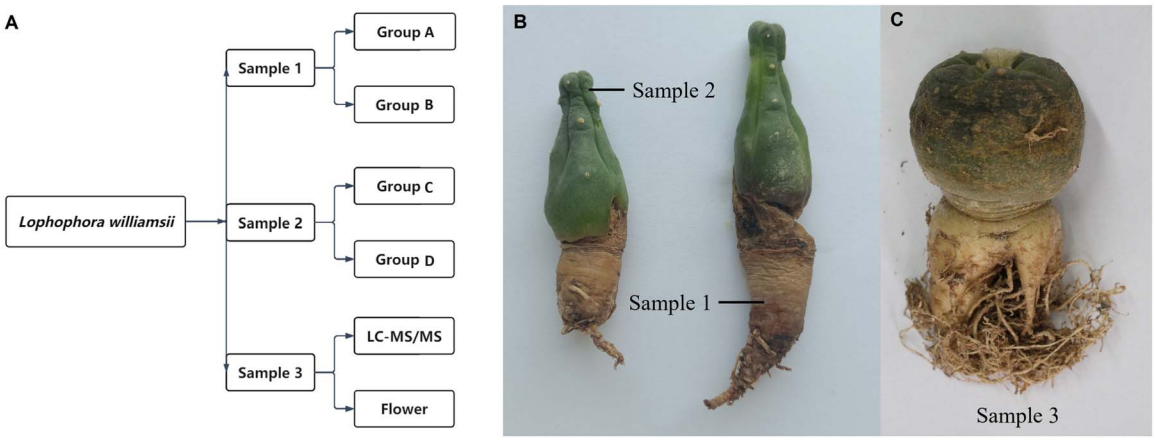

Figure 1. Flow chart of plant sample grouping (A); *Lophophora williamsii* Sample 1 and Sample 2 (B); and Sample 3 (C).

Table 1. Treatment methods, storage conditions, and section parameters of the different samples.

Sample	Group	Treatment methods	Storage conditions	Embedding	Slice thickness (μm)	Slice temperature
Lophophora williamsii	A	Dry in a vacuum oven at 60°C for 4 h	–	Paraffin	8	Normal atmospheric temperature
	B	Dry in a vacuum oven at 60°C for 24 h	Normal atmospheric temperature	–	–	–
	C	Quickly freezing in liquid nitrogen	−80°C	Over-the-counter solution	10, 20, 30, 40, 50	−60°C, −40°C, −20°C, −10°C
	D	Quickly freezing in liquid nitrogen	−80°C	Gelatin	10, 20, 30, 40, 50	−60°C, −40°C, −20°C, −10°C

over-the-counter (OTC) solution (100 mg/mL) and gelatin in tinfoil embedding boxes filled, respectively, and then frozen at −80°C for 2 min to obtain frozen blocks for sectioning. The most suitable slice thickness was determined by cutting the sample cube at thicknesses of 10, 20, 30, 40, and 50 μm using a cryostat (Leica CM1950 Platform, Wetzlar, Germany). The sections were attached to the surface of the ITO-coated conductive glass slides and transferred to a vacuum oven at room temperature for 15 min for moisture evaporation prior to optical imaging and application of the matrix. The optimum slice temperature was determined by slicing the sample cube at a slice thickness of 40 μm at temperatures of around −60°C, −40°C, −20°C, and −10°C.

The dry sepals and petals were pasted onto the surface of ITO-coated conductive glass slides with double-sided carbon conductive tape.

Matrix selection and spraying

Eight matrices (DHB, CHCA, S-DHB, DT, DCTB, 1,5-DAN, 9-AA, and 2,5-DHAP) were tested to screen for an optimum matrix. A 1 μL drop of mescaline standard solution (10 μg/mL) was spotted onto the stainless steel MALDI target plate, allowed to dry, and then covered with 1 μL of the desired matrix (10 mg/mL) to obtain cocrystals. After air drying, the target plate was placed into the iMScope for analysis.

The results of the optimal matrix selection identified DCTB as the best matrix for experimental spraying. An 800-μL volume of the DCTB matrix solution was added to the cavity of an artist's airbrush (MR Linear Compressor L7/PS270 Airbrush, Tokyo, Japan) and used to spray the matrix uniformly onto the surface of the samples on the slides. The distance between the tip of the airbrush and the tissue surface was about 8 cm. After spraying, the samples were left at room temperature for 5 min to vaporize the solvent. The samples were then ready for data collection.

Sample preparation for LC–MS/MS analysis

The petal and sepal samples that were imaged by mass spectrometry were micropunched [44] using a 0.5-mm diameter aluminum punch kit (#69033–05, Electron Microscopy Sciences, Hatfield, PA, USA). The punches were placed in 1.5 mL centrifuge tubes, and 500 μL MeOH was added. Then the tubes were sonicated for 60 min. After sonication, each extract was passed through a 0.22 μm filter membrane, and 5 μL of the filtrate was injected into the LC–MS/MS.

The *L. williamsii* Sample 3 was microsampled from five different positions: three samples from the crown and two samples from the subterranean stem. Each sampled section was separated into epidermal and fleshy tissues, weighed with a precision balance (Cubis II Micro Balance, Sartorius, Germany), and placed into a 2 mL tube containing ceramic beads. A 40-μL volume of IS (10 ng/mL) and 660-μL MeOH were then added, and the samples were pulverized in a JXFSPRP-CLN freeze-grinder (Shanghai Jing Xin Industrial Development Co., Ltd, Shanghai, China) under the following conditions: temperature: −35°C; speed: 2 500 rpm; run time: 40 s; interval time: 60 s; number of repetitions: 15 cycles; and grinding speed: 18 m/s. The mixture was ultrasonicated

for 10 min and then centrifuged at 13 500 rpm for 5 min. After centrifugation, the supernatant was filtered through a 0.22 μm filter membrane (Sinopharm Chemical Reagent Co., Ltd, Shanghai, China) and then 5 μL of the filtrate was injected into the LC–MS/MS system for analysis.

Instrument conditions and analysis

MALDI-MSI

Laser intensity

For mescaline analysis, the instrument was operated in positive/negative mode, and spectra were acquired in the range of *m/z* 50–400. The most suitable laser intensity was determined by testing laser intensities of 15, 20, 25, 30, 35, 40, 45, 50, 55, and 60. The laser was calibrated with ink, and an accurate mass was ensured by calibrating the MSI instrument with the DHB matrix before each experiment. All acquired data were analyzed using IMAGEREVEAL MS software (Shimadzu, Kyoto, Japan). The same software was used for visualization and relative quantitative analysis.

Other parameters

All MSI data were acquired on an iMScope QT (Shimadzu), which has an integrated optical microscope (magnification ×5, ×10, ×40), an atmospheric pressure MALDI source, and a quadrupole time-of-flight analyzer. The scanning area was determined using an optical microscope, and the sample slices were irradiated with a diode-pumped 355 nm Nd:YAG laser using the following parameters: laser shots, 200; repetition rate, 2 000 Hz; laser diameter, 0 (5 μm); detector voltage, 2.4 kV; and pitch, 30 μm.

Region of interest semi-quantitative analysis

The region of interest (ROI) semi-quantitative function of IMAGEREVEAL MS software (https://www.ssi.shimadzu.com/products/life-science-lab-instruments/imaging/imagereveal-ms/index.html) was used to draw the area at the micropunched location with the same size as the aperture. Each ROI contained 150 pixels, even if the shape of the drawn area was different. The value of each ROI showed the relative intensity of the average spectrum (pixel by pixel) of mescaline produced by MALDI-MSI analysis in a given region. Manually drawn ROIs were located at different locations within the crown section, with each ROI containing 450 pixels.

LC–MS/MS

The LC–MS/MS system consisted of a Sciex 6500 Q-trap™ quadrupole mass spectrometer (AB Sciex, Foster City, CA, USA) operated in the positive electrospray ionization and multiple reaction monitoring modes and coupled to an Acquity™ Ultra Performance LC (Waters Corporation, Milford, MA, USA). Data acquisition and quantification were performed using Analyst 1.6.3 (https://download.sciex.com/Analyst_1.6.3_RelNotes.pdf) and MultiQuant 3.0.2 software (https://download.sciex.com/MultiQuant_302_Software_Release_Notes.pdf). The mobile phase consisted of a mobile phase A (0.1% formic acid in water) and a mobile phase B (ACN) at a flow rate of 0.25 mL/min using the following binary gradient: 5% B/95% A (v/v) at 0 min, held at 5% B until 0.5 min, linear gradient to 15% B from 0.5 to 1 min, held at 15% B between 1 and 2 min, and a linear gradient to 50% B from 2 to 2.5 min, held at 50% B between 2.5 and 4 min, and returned to the initial composition at 5 min. An ACQUITY UPLC BEH C18 column (2.1 mm × 100 mm, 1.7 μm i.d., Waters) was used for chromatographic separation. The injection volume for all samples was 5 μL. The autosampler temperature was held at 4°C, and the autosampler needle was washed thoroughly between injections. The optimum mass spectra were obtained under the following conditions: curtain gas, 30 psi (nitrogen); ion spray voltage, 5 500 V; collision cell exit potential, 13 V; entrance potential, 10 V; collision activation dissociation gas, middle; ion source gas, 35 psi; ion source gas 2, 40 psi; and source temperature (TEM), 500°C.

Mescaline was determined using a previously published LC–MS/MS method [45]. The retention time of mescaline was 2.75 min. The assay validated mescaline with a limit of detection of 3 pg/mg. The response was linear over a concentration range of 10–1 000 pg/mg, the intraday precision RSD values were < 8.8%, and the interday precision RSD values were between 1.6% and 8.8%. The intraday and interday accuracy was 88.8%–108.8%.

Results and discussion

Method optimization

Optimization of preservation

The results for four different preservation methods for *L. williamsii* are shown in Table 2. For fresh plants, the samples of Group B gradually shrank as the drying time progressed, which was caused by moisture loss [46], and this was not conducive to subsequent slicing. Preserving the original shape of the sample as much as possible is important, as this is the basis of *in situ* analysis. However, the samples of Groups A, C, and D maintained their original morphology, and the samples of Groups C and D had better morphology. In addition, research has shown that samples can be stored frozen at −80°C for at least 1 year without significant degradation [47]; therefore, the method of −80°C cryopreservation after liquid nitrogen freezing was ultimately selected in the present study. Freezing of freshly cut samples in plastic tubes should be avoided, as the samples are very likely to adhere to the sides of the tube or even take on the shape of the tube.

Table 2. Sample storage effects after different treatment methods and storage conditions.

Sample	Group	Appearance	Storage results
Lophophora williamsii	A	Slight dehydration can roughly maintain the original shape	Can be sliced
	B	Completely dehydrated, wrinkled and brittle, unable to maintain the original shape	Unable to slice
	C	Maintain the original shape	Can be sliced
	D	Maintain the original shape	Can be sliced

Optimization of sections of plants

As shown in Table 3, the use of paraffin or OTC as the embedding medium prevented the detection of the target signal when the tissues were directly sectioned for MSI, but the target was detected when gelatin was used for embedding. We considered that the paraffin or OTC might have adhered to the sample surface with the movement of the slicer, resulting in interference or affecting the combination of matrix and sample, as also mentioned by Goodwin [33]. Dewaxing and rinsing the samples with water did not restore the ability to detect the target signal. The process of paraffin removal can possibly modify or remove endogenous components (such as proteins, peptides, lipids, or low molecular weight substances) in tissue samples [30]. Some researchers have indicated that contamination by OTC could cause severe suppression of the detection of target compounds [48] because they can ionize readily and act as ion suppressors [49]. The contamination by OTC can be effectively removed by a water wash after the ethanol fixation wash steps [50], but we did not use ethanol as a wash because the standard solution of mescaline is usually prepared in methanol, and ethanol washing also takes away part of the target. For these reasons, we finally chose the gelatin embedding method. If enough samples are available, water (ice) can be used as the embedding medium if complete embedding is essential [51].

The choice of the thickness of the frozen section is the first consideration, as a thinner section will provide a more sensitive detection of ions [21] and a clearer image of the cell structure without stacking when observed under the microscope [48]; it will also require a shorter air-drying time. However, a thinner section will have a greater brittleness, making the operation very difficult. A thicker section is easier to handle and can provide a more complete picture of the tissue, especially for samples with a large area. However, it may also increase the formation of cell cavities caused by ice crystals and potentially limit the detection of analytes by MALDI due to the insulating effect between the tissue surface and the conductive slide [33]. Table 4 shows the optimization of the thickness of the frozen slices in a range from 10 to 50 μm. The rigid structure of the plant cell wall, the high water content of cells, and the presence of large or if the samples can be sectioned in the frozen state without embedding. vacuoles make frozen sections of most plant tissues difficult to handle and easily rupture [52]. An increase in thickness makes the slice less likely to wrinkle and more likely to maintain its original shape. The success rate of plant sections is essentially the same when the section thickness is 40 and 50 μm, but thicker insulation samples may adversely affect the performance of the mass analyzer [53, 54]. Based on these considerations, and combined with the slice morphology and success rate obtained with actual slices, we ultimately chose a slice thickness of 40 μm, although a thickness of 10–20 μm has been suggested as the best option for maximizing the signal-to-noise ratio [51].

The next consideration was the choice of slicing temperature. The sample was kept frozen at −80°C. If the sample is removed from the freezer and sliced directly, the temperature is too low and the slice is likely to curl and break. If the sample is left for too long after being removed from the freezer, the temperature becomes too high and the slice is likely to wrinkle. The experiments in Table 5 show that satisfactory results can be obtained at a temperature of about −20°C, which is a typical slice temperature ranging from −16 to −26°C [33]. In addition, the rocking handle of the microtome should be rotated with a continuous and uniform force. Once a sample section has been transferred to a slide, the target within the section is susceptible to photodegradation. To minimize this effect, the section should be kept in a dark environment before analysis. Figure 2 shows the optical images of *L. williamsii* (Group D) sections of 40 μm thickness made at −20°C.

Optimization of the MALDI conditions

Optimization of the matrix

The optimal matrix was selected based on the signal of a 10 μg/mL mescaline standard solution when different matrices were used. Each matrix has three parallel samples. In positive ion mode, the predominant mescaline-related ion ($[M+H]^+$ at *m/z* 212.1282 (which has a mass deviation of 0.47 ppm from the theoretical value of *m/z* 212.1281) could be detected with the DT, S-DHB, and DCTB matrices with average signal intensities of 206.3, 183.6, and 5 043.3, respectively. By contrast, the target signal was not detected

Table 3. Imaging effects of *Lophophora williamsii* embedded with different methods.

Sample	Group	Embedding	Imaging effect	Treatment after embedding slice	Imaging effect
Lophophora williamsii	A	Paraffin	No target signal	Dewaxed and dehydrated with xylene and ethanol	No target signal
	B	–	–	–	–
	C	Over-the-counter solution	No target signal	Rinsed with water	No target signal
	D	Gelatin	High signal	–	–

Table 4. Effect of slice thickness on slice morphology and slice success rate (*Lophophora williamsii* sample from Group D).

Slice thickness (μm)	Slice morphology	Slice success rate (%)
10	Severe wrinkling	<10
20	Most wrinkling	<30
30	Slight wrinkling	<50
40	Basically maintain the original form	>60
50	Basically maintain the original form	>60

Table 5. Effect of slice temperature on slice morphology and slice success rate (*Lophophora williamsii* sample from Group D).

Slice temperature (°C)	Slice morphology	Slice success rate (%)
−60	Severe breaking	<10
−40	Slight breaking	<50
−20	Basically maintain the original form	>60
−10	Wrinkling	<50

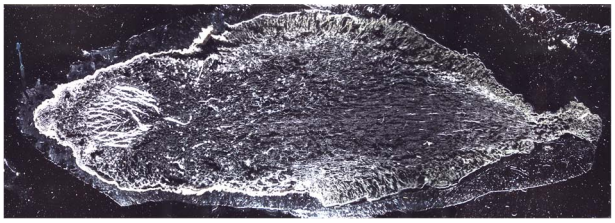

Figure 2. An optical image of *Lophophora williamsii* Sample 2 (Group D) slice with a thickness of 40 μm made at a temperature of −20°C.

with DHB, CHCA, 9-AA, 1,5-DAN, or 2,5-DHAP as matrices (Figure 3A).

The uniform deposition and crystal size of the matrix on the tissue surface are very important for obtaining high-quality images. The presence of small and homogeneous matrix crystals can improve the sensitivity and spatial resolution of MALDI-MSI [55–58]. This is because, in the MALDI process, the laser energy is easily dissipated in large crystals, resulting in preferential ionization of high-abundance or high-polarity components. This causes a signal suppression effect on low-abundance or low-ionization species. By contrast, for small crystals, the low energy transfer efficiency between adjacent crystals reduces the dissipation of laser energy, thereby providing greater potential for the ionization/desorption of analytes in the crystal [59]. As shown in Figure 4, samples with DHB, 9-AA, 1,5-DAN, and 2,5-DHAP matrices had larger crystals. In addition, 9-AA, 1,5-DAN, and 2,5-DHAP were more suitable matrices for the negative ion mode [60, 61]. Although the crystallinity of the CHCA matrix is small, the large number of matrix-related ions generated during laser irradiation can mask the signal of the analyte, making CHCA unsuitable for MALDI analysis of low molecular weight analytes [60]. The performance of DT in this study is not satisfactory. We also didn't find any references. Some studies have shown that the use of the S-DHB matrix (a mixture of DHB and 2-hydroxy-5-methoxybenzoic acid at a ratio of 9:1) can significantly improve the spectrum and improve the quality accuracy [62]. Our results also show that S-DHB has a better matrix-assisted effect than DHB alone. However, compared with DCTB, the matrix enhancement effect of S-DHB is still insufficient.

The mass spectrum is very "clean" when using DCTB as a matrix because of the low number of matrix clusters due to the intrinsic nature of the matrix. DCTB also has a relatively neutral pH value, which causes less damage to proton-sensitive compounds, thereby reducing the spectral complexity to a certain extent [56]. Note that in the present study, when preparing the matrix solution for the actual sample, DCTB was completely dissolved in DCM. However, because DCM is highly volatile, ACN was added to prevent the matrix particles from blocking the spray gun head due to too rapid solvent volatilization during spraying.

Optimization of laser intensity

The laser intensity for the mescaline standard solution was optimized using DCTB as the matrix. Each laser intensity has three parallel samples. As shown in Figure 3B, when the laser intensity (also referred to as power density or irradiance) was 15, 20, 25, 30, 35, 40, 45, 50, 55, or 60, the intensity of the mescaline peak at *m/z* 212.1282 varied with the laser intensity. At laser intensities of 15–50, the signal intensity for mescaline increased with increasing laser intensity and reached a peak at 50. At a laser intensity greater than 50, the signal strength of mescaline began to decrease. When the laser intensity was 45 and 50, the signal strength of *m/z* 212.1282 showed little difference, with an average of 5 532.3 and 5 723.3, respectively. However, the laser intensity of 50 produced very strong signal interference due to background noise. Therefore, a laser intensity of 45 was selected as optimal. The mass spectra of 10 μg/mL mescaline standard solution when DCTB

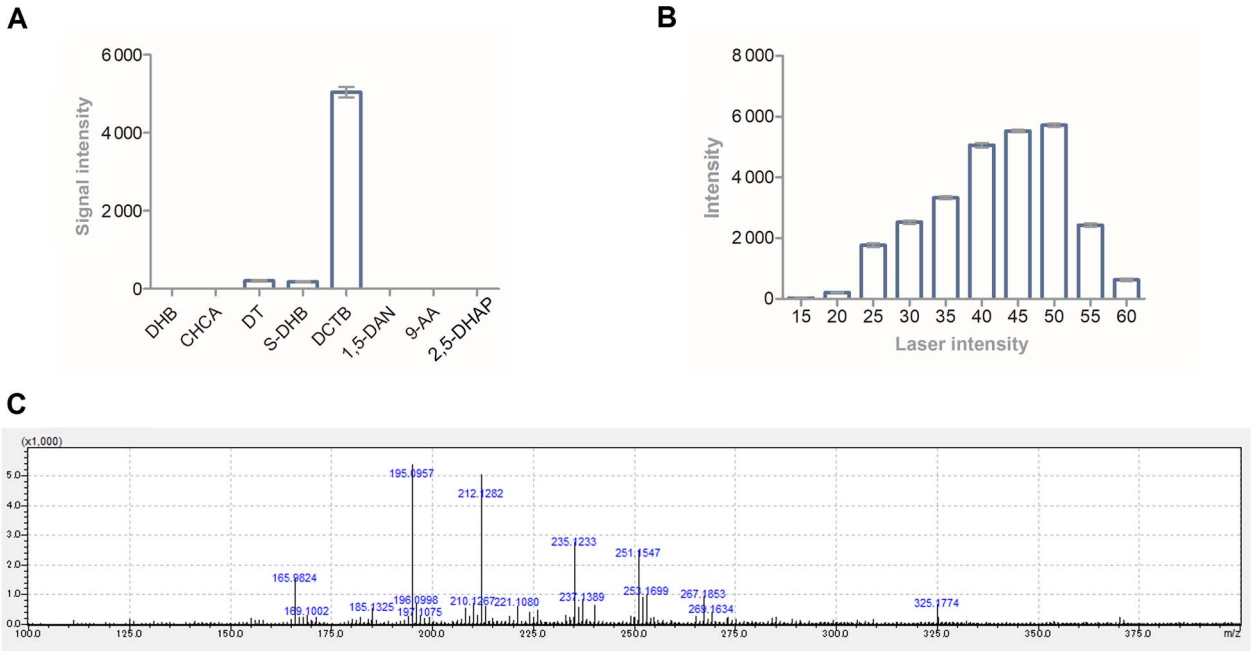

Figure 3. (A) Signal intensity of a 10 μg/mL mescaline standard solution when DHB, CHCA, DT, S-DHB, DCTB, 1,5-DAN, 9-AA, and 2,5-DHAP were used as matrices. (B) The intensity of a 10 μg/mL mescaline standard solution under different laser intensities. (C) The mass spectra of 10 μg/mL mescaline standard solution when DCTB was used as a matrix, and the laser intensity was 45.

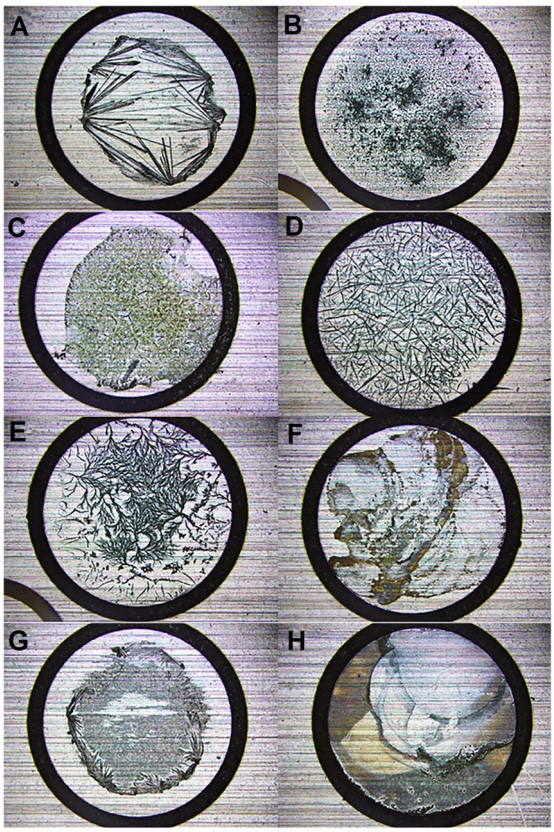

Figure 4. Optical photographs (10×) of prepared sample spots of 10 μg/mL mescaline standard solution with matrices of (A) DHB, (B) CHCA, (C) 9-AA, (D) 1,5-DAN, (E) 2,5-DHAP, (F) DCTB, (G) S-DHB, and (H) DT.

is used as a matrix and the laser intensity is 45 are shown in Figure 3C.

In MALDI-MSI, desorption/ionization is realized in a complex process initiated by a single laser. The solid mixture containing analytes and matrix molecules is irradiated by laser pulses, and then a large number of neutral particles and ions are released from the sample surface into the gas phase [63, 64]. The physicochemical properties of the laser (e.g. wavelength, pulse duration, fluence, and beam profile) are key factors for achieving high analytical sensitivity. This is because even when the ion yield is relatively low, as long as sufficient material can be sampled and the analyte ion signal remains stronger than the background noise with the increased number of laser pulses, a high ion signal per laser pulse can eventually be achieved [65].

The increase in the ion signal intensity of the analyte is also limited. At a low laser intensity, the so-called laser desorption regime applies, but when a high laser intensity is used, the number of ions decreases with the irradiance [66]. This is because the ion concentration increases at high laser intensity, and the formation of ion–ion recombinations will limit any further increase in the ion intensity [67].

MSI and verifiable LC–MS/MS results

MALDI-MSI of mescaline in L. williamsii

The software compared the actual sample with the standard solution and it reported the hits with a mass error window of 5 ppm, which was verified using intelligent exact mass interpretation of the mass spectrum acquired [68, 69]. The ions of *m/z* 212.12758 from the MALDI-MSI analysis in the positive ion mode were identified as the mescaline in *L. williamsii*. For plant slices in Figure 5, the mean signal intensity of mescaline of two ROIs on the epidermal tissue of subterranean stem was 27 519.1 ± 1 677.7 and on the fleshy tissue of subterranean stem was 16 954.9 ± 3 624.2, the mean signal intensity of mescaline of three ROIs on the epidermal tissue of crown was 40 368.3 ± 6 839.0 and on the fleshy tissue of crown was 16 335.1 ± 7 484.8, the mean signal intensity of mescaline of five ROIs on the epidermal tissue was 35 228.6 ± 8 621.1 and on the fleshy tissue was 16 583.1 ± 5 604.5. The mescaline content was higher in epidermal tissue than in fleshy tissue (paired-sample *t*-test, $P < 0.05$). Further analysis of the distribution of mescaline in the crown of *L. williamsii* is shown in Figure 6D. The mean signal intensity of mescaline of eight ROIs where meristem was concentrated (the upper part of the crown) was 78 246.5 ± 11 984.7, while the mean signal intensity of eight ROIs on the rest of the crown was 62 523.3 ± 7 362.6. The mescaline content was higher in meristems of the crown than in the other parts of the crown (independent sample *t*-test, $P < 0.05$).

Reliability verification of MSI results

The accuracy of the MSI results was determined by comparing the ROI semi-quantitative data of the MSI results with LC–MS/MS data. Each micropunched point has two values: the LC–MS/MS peak area/average concentration and the ROI signal intensity. The one-to-one relationship between these two variables was used to fit a curve and calculate the coefficient of determination. Figure 5 shows that, for the same samples (petals and sepal), the coefficient of determination R^2 value can be as high as 90%, and for different samples, the fitting degree was about 60%.

The LC–MS/MS method has a high degree of accuracy, authenticity, and sensitivity [70–72]. The results for MSI and LC–MS/MS were quantitatively uniform because when the coefficient of determination R^2 is close to 1, the two variables are considered to be highly correlated, and the reference value of the related equation is higher. For the same sample, the high fitting degree not only shows the authenticity of MALDI results, but it also shows the feasibility of using preprocessing methods and MALDI optimization conditions. For different samples, the high degree of fitting represents the generality of the experimental results.

Description & sampling proposal based on spatial distribution

Based on the results of this study, the top part of the crown was the largest enrichment area for mescaline in *L. williamsii*, which was consistent with our previous results [17]. In previous studies, we discussed the possible mechanism by which this phenomenon occurs: (i) defensive compounds are found at high levels in vulnerable parts of the plant to build up defenses against foragers; (ii) The mescaline synthetic pathway occurs mainly in neonatal cells, so mescaline is concentrated in areas with dense meristem. If this hypothesis is correct, defensive compounds, such as mescaline, should be found at the highest concentrations in areas of high productivity and potential reproduction among similar cactus plants. This result also has wide applicability to extrapolation to other plants. For example, in cannabis plants, Δ^9-tetrahydrocannabinol (THC) is concentrated in the flowers and robust leaves (shoots) [73–75]; for opioids, the alkaloids are localized predominantly within the walls and

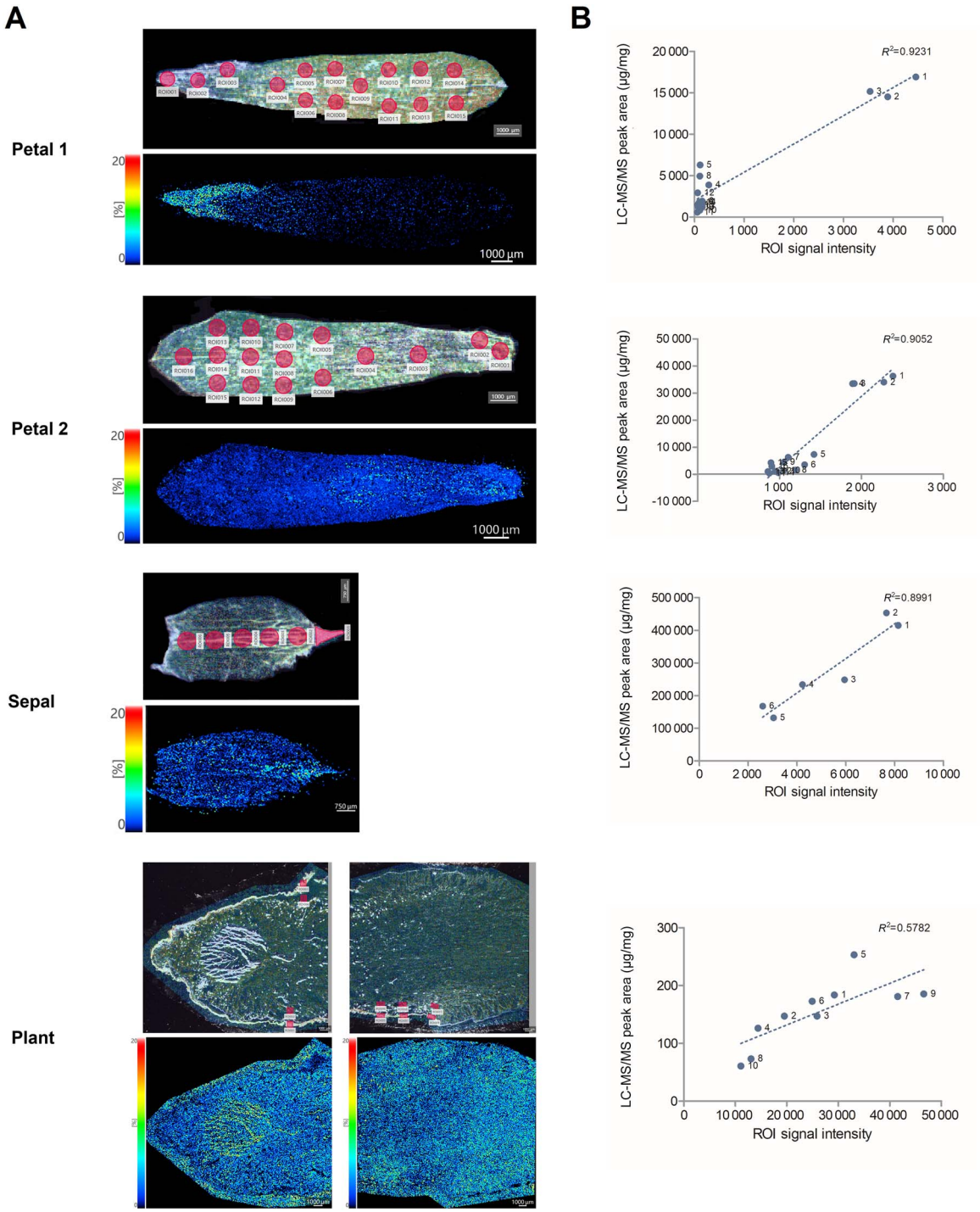

Figure 5. (A) Comparison of micropunches and region of interest (ROI) semi-quantitative regions with mass spectrometry imaging (MSI) in different parts of *Lophophora williamsii* samples. (B) Fitted curve corresponding to different positions.

vascular bundles of the capsules of *Papaver setiferum*, with the highest relative abundances occurring in the lower half of the capsules, toward the peduncle [76]. Tryptamines, represented by *N*,*N*-dimethyltryptamine, accumulate in tissues such as bark that forms a defensive epidermis and carries out important nutrient transport [77, 78]. Therefore, from the perspective of zero tolerance control, the reproductive organs and robust tissues of seized suspicious plants can be given priority as sampling regions. These regions are likely to have rich concentrations of targeted compounds, which means that not only will the requirements for detection sensitivity be reduced, but obtaining relevant evidence of the presence of illegal compounds in the seized plant samples will be easier.

From another point of view, in this study, the mescaline content in the epidermal tissues of *L. williamsii* was about twice that of the fleshy tissues, and the mescaline content in the crown meristem was about 1.25 times that of other tissues. Similar results were obtained in the previous study, as the mescaline content in the epidermal tissues was about 1.64 times that in fleshy tissues, and the content in the crown meristem was about 1.5 times that in other tissues. Other results and ours suggest that mescaline concentrations vary at

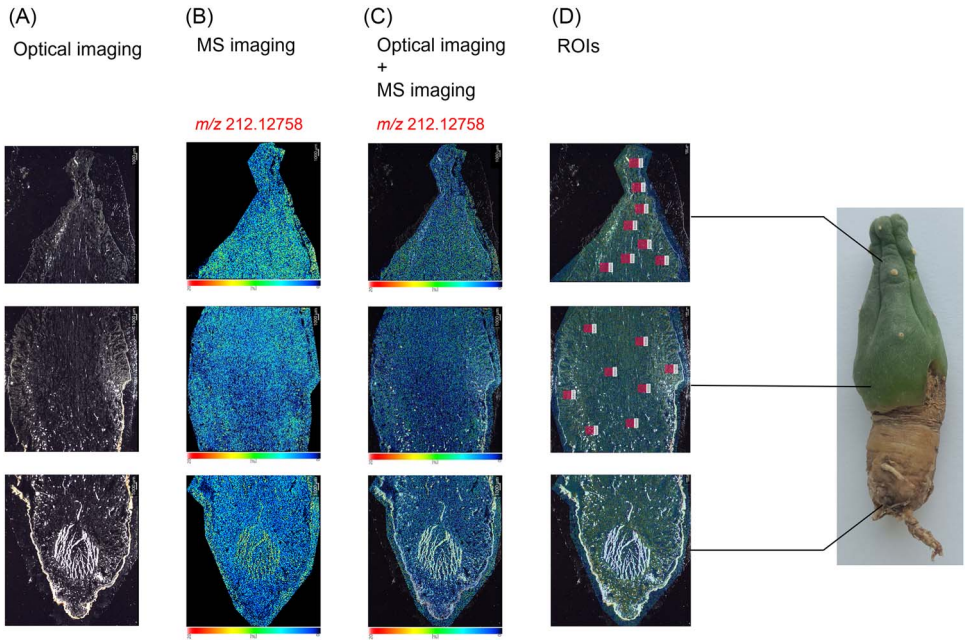

Figure 6. Matrix-assisted laser desorption/ionization mass spectrometry imaging (MALDI-MSI) analysis of mescaline in positive ion mode in *Lophophora williamsii* Sample 2 (Group D). (A) Optical imaging. (B) Mass spectrometry (MS) imaging (*m/z* 212.12758, $[M+H]^+$). (C) Optical and MS overlay imaging (*m/z* 212.12758, $[M+H]^+$). (D) Region of interest (ROI) semi-quantitative regions on the crown of *L. williamsii*.

different locations in the plant [79–81]. Therefore, a comprehensive consideration is needed for the risk of *L. williamsii* as a whole plant. During sampling, samples from several parts of the plant should be collected, and the distribution differences of target compounds at different locations should be taken into account to evaluate the harmfulness of the whole plant itself. A potent mescaline intoxication is ~3.75 mg/kg body weight [38], and mescaline has the lowest potency of the known orally active, naturally derived hallucinogens [82]. Given the cultivation situation, stating whether all *L. williamsii* or related plants are at risk of being addictive or dangerous is difficult. In addition, because cacti are common ornamental plants, *L. williamsii* is not subject to drug regulations in some countries or regions; therefore, seeds can be legally purchased and grown in greenhouses alongside other plants without being detected [83]. In this context, consideration should be given to the total amount of mescaline available, as this might be a better basis for assessing violations.

Conclusions

In conclusion, a high spatial resolution MALDI-MSI analysis method was developed for the study of mescaline in fresh succulent plants and successfully applied to real samples. As a preferred solution, low-temperature storage at −80°C and drying tissues as "bookmarks" are recommended as suitable storage methods, and slicing thicknesses of 40 μm, cut at −20°C, are acceptable for processing succulent samples. In addition, laser intensity and auxiliary matrix are specific parameters worth optimizing for the analysis of different target compounds. The ROI semi-quantitative analysis revealed that mescaline was concentrated in the epidermal tissue of the plant, as well as in the meristematic tissues of the crown, which is in good agreement with the quantitative results of the spatial distribution of LC–MS/MS. Based on the results of our analysis, when the principle of "zero tolerance" is followed, we suggest that when handling plant samples that may contain drugs, the robust and active tissue areas and areas where reproductive organs are located should be given priority. If other factors need to be taken into account, multi-site sampling is the recommended sampling proposal based on the results of spatial distribution.

Acknowledgements

Thanks for the support by the Key Laboratory of Forensic Science of Ministry of Justice, Shanghai Science and Technology Commission and the Science and Technology Commission of Shanghai Municipality [21DZ2270800/19DZ2292700].

Authors' contributions

Jiaman Lin participated in all the experimental analysis and drafted the manuscript. Keming Yun was responsible for review and editing. Qiran Sun was responsible for conceptualization. Ping Xiang was responsible for conceptualization, supervision, and funding acquisition. Lina Wu was responsible for resources and investigation. Shuo Yang participated in LC–MS/MS analysis. Junling Dun participated in MALDI-MSI analysis. Hang Chen and Shanlin Fu conceived of the study, and participated in its design and coordination and helped to draft the manuscript. All authors contributed to the final text and approved it.

Compliance with ethical standards

The article did not involve work with human participants or animals requiring ethical clearance by the authors. The Ethics Committee of the Academy of Forensic Science approved the use of the sample and the study.

Disclosure statement

Ping Xiang initial holds the position of Editorial Board Member for *Forensic Sciences Research* and is blinded from reviewing or making decisions for the manuscript.

Funding

This study was supported by grants from the National Key R&D Program of China [Grant No. 2022YFC3302005] and Natural Science Foundation of Shanghai [Grant No. 19ZR1478500].

References

1. Global overview drug demand drug supply. The world drug report. 2022. https://www.unodc.org/res/wdr2022/MS/WDR22_Booklet_2.pdf
2. The challenge of new psychoactive substances. A report from the Global SMART Programme. 2013. https://www.unodc.org/documents/scientific/NPS_2013_SMART.pdf
3. Li S, Zhu N, Tang C, et al. Differential distribution of characteristic constituents in root, stem and leaf tissues of salvia miltiorrhiza using MALDI mass spectrometry imaging. Fitoterapia. 2020;146:104679.
4. Dashbaldan S, Rogowska A, Pączkowski C, et al. Distribution of triterpenoids and steroids in developing rugosa rose (*Rosa rugosa* Thunb.) accessory fruit. Molecules. 2021;26:5158.
5. Zhang JZ, Wang C, Zhu TT, et al. Spatial distribution, antioxidant capacity, and spore germination-promoting effect of bibenzyls from *Marchantia polymorpha*. Antioxidants. 2022;11:2157.
6. Neumann EK, Djambazova KV, Caprioli RM, et al. Multimodal imaging mass spectrometry: next generation molecular mapping in biology and medicine. J Am Soc Mass Spectrom. 2020;31: 2401–2415.
7. Yan H, Xiang P, Shen M. Current status of hair analysis in forensic toxicology in China. Forensic Sci Res. 2021;6:240–249.
8. Amstalden van Hove ER, Smith DF, Heeren RM. A concise review of mass spectrometry imaging. J Chromatogr A. 2010;1217: 3946–3954.
9. Boughton BA, Thinagaran D, Sarabia D, et al. Mass spectrometry imaging for plant biology: a review. Phytochem Rev. 2016;15: 445–488.
10. Mellinger AL, Muddiman DC, Gamcsik MP. Highlighting functional mass spectrometry imaging methods in bioanalysis. J Proteome Res. 2022;21:1800–1807.
11. Zaima N, Hayasaka T, Goto-Inoue N, et al. Matrix-assisted laser desorption/ionization imaging mass spectrometry. Int J Mol Sci. 2010;11:5040–5045.
12. Balluff B, Schöne C, Höfler H, et al. MALDI imaging mass spectrometry for direct tissue analysis: technological advancements and recent applications. Histochem Cell Biol. 2011;136:227–244.
13. Kamanna S, Henry J, Voelcker N, et al. "Bottom-up" *in situ* proteomic differentiation of human and non-human haemoglobins for forensic purposes by matrix-assisted laser desorption/ionization time-of-flight tandem mass spectrometry. Rapid Commun Mass Spectrom. 2017;31:1927–1937.
14. Erne R, Bernard L, Steuer AE, et al. Hair analysis: contamination versus incorporation from the circulatory system-investigations on single hair samples using time-of-flight secondary ion mass spectrometry and matrix-assisted laser desorption/ionization mass spectrometry. Anal Chem. 2019;91:4132–4139.
15. Vandenbosch M, Nauta SP, Svirkova A, et al. Sample preparation of bone tissue for MALDI-MSI for forensic and (pre)clinical applications. Anal Bioanal Chem. 2021;413:2683–2694.
16. Jiang Y, Sun J, Huang X, et al. Direct identification of forensic body fluids by MALDI-MS. Analyst. 2019;144:7017–7023.
17. Lin J, Yang S, Ji J, et al. Natural or artificial: an example of topographic spatial distribution analysis of mescaline in cactus plants by matrix-assisted laser desorption/ionization mass spectrometry imaging. Front Plant Sci. 2023;14:1066595.
18. Benyahia H, Ouarti B, Diarra AZ, et al. Identification of lice stored in alcohol using MALDI-TOF MS. J Med Entomol. 2021;58: 1126–1133.
19. Lukowski JK, Pamreddy A, Velickovic D, et al. Storage conditions of human kidney tissue sections affect spatial lipidomics analysis reproducibility. J Am Soc Mass Spectrom. 2020;31:2538–2546.
20. Reeve MA, Stewart H, Ryan MJ. MALDI-TOF MS spectral variation is observed between fungal samples grown under identical conditions after long-term storage by cryopreservation, freeze-drying, and under oil. Cryo Lett. 2019;40:145–151.
21. Nie LX, Dong J, Huang LY, et al. Microscopic mass spectrometry imaging reveals the distribution of phytochemicals in the dried root of *Isatis tinctoria*. Front Pharmacol. 2021;12:685575.
22. Kawamoto T, Kawamoto K. Preparation of thin frozen sections from nonfixed and undecalcified hard tissues using Kawamoto's film method (2020). Methods Mol Biol. 2021;2230: 259–281.
23. Luczak M, Marczak L, Stobiecki M. Optimization of plasma sample pretreatment for quantitative analysis using iTRAQ labeling and LC-MALDI-TOF/TOF. PLoS One. 2014;9:e101694.
24. Sato H, Nakamura S. Development of an on-plate sample pretreatment for MALDI-TOF-MS measurements and its application to the analysis of organic industrial products. Bunseki Kagaku. 2018;67: 281–291.
25. Chen Y, Tang W, Gordon A, et al. Development of an integrated tissue pretreatment protocol for enhanced MALDI MS imaging of drug distribution in the brain. J Am Soc Mass Spectrom. 2020;31: 1066–1073.
26. Enthaler B, Pruns JK, Wessel S, et al. Improved sample preparation for MALDI–MSI of endogenous compounds in skin tissue sections and mapping of exogenous active compounds subsequent to *ex-vivo* skin penetration. Anal Bioanal Chem. 2012;402: 1159–1167.
27. Bien T, Bessler S, Dreisewerd K, et al. Transmission-mode MALDI mass spectrometry imaging of single cells: optimizing sample preparation protocols. Anal Chem. 2021;93:4513–4520.
28. Briggs MT, Ho YY, Kaur G, et al. N-glycan matrix-assisted laser desorption/ionization mass spectrometry imaging protocol for formalin-fixed paraffin-embedded tissues. Rapid Commun Mass Spectrom. 2017;31:825–841.
29. Kelley AR, Colley M, Dyer S, et al. Ethanol-fixed, paraffin-embedded tissue imaging: implications for Alzheimer's disease research. J Am Soc Mass Spectrom. 2020;31:2416–2420.
30. Hermann J, Noels H, Theelen W, et al. Sample preparation of formalin-fixed paraffin-embedded tissue sections for MALDI-mass spectrometry imaging. Anal Bioanal Chem. 2020;412:1263–1275.
31. Dos Santos NA, de Almeida CM, Gonçalves FF, et al. Analysis of *Erythroxylum coca* leaves by imaging mass spectrometry (MALDI-FT-ICR IMS). J Am Soc Mass Spectrom. 2021;32:946–955.
32. Wang J, Wang C, Han X. Enhanced coverage of lipid analysis and imaging by matrix-assisted laser desorption/ionization mass spectrometry via a strategy with an optimized mixture of matrices. Anal Chim Acta. 2018;1000:155–162.
33. Goodwin RJA. Sample preparation for mass spectrometry imaging: small mistakes can lead to big consequences. J Proteomics. 2012;75:4893–48911.
34. Li H, Wu R, Hu Q, et al. A matrix sublimation device with an integrated solvent nebulizer for MALDI-MSI. J Am Soc Mass Spectrom. 2022;33:11–16.
35. Tressler C, Tilley S, Yang E, et al. Factorial design to optimize matrix spraying parameters for MALDI mass spectrometry imaging. J Am Soc Mass Spectrom. 2021;32:2728–2737.
36. Nishikaze T, Takayama M. Disappearance of interfering alkali-metal adducted peaks from matrix-assisted laser desorption/ionization mass spectra of peptides with serine addition to alpha-cyano-4-hydroxycinnamic acid matrix. Rapid Commun Mass Spectrom. 2007;21:3345–3351.

37. Terry M, Steelman KL, Guilderson T, et al. Lower Pecos and Coahuila peyote: new radiocarbon dates. J Archaeol Sci. 2006;33: 1017–1021.
38. Halpern JH. Hallucinogens and dissociative agents naturally growing in the United States. Pharmacol Ther. 2004;102:131–138.
39. Cengisiz C, Bal U, Ulutas K, et al. Mescaline abuse via peyote cactus: the first case report in Turkey. Anadolu Psikiyatri Dergisi. 2016;17:68.
40. Gołembiowska K, Jurczak A, Kamińska K, et al. Effect of some psychoactive drugs used as "Legal Highs" on brain neurotransmitters. Neurotox Res. 2016;29:394–407.
41. da Cunha KF, Oliveira KD, Huestis MA, et al. Screening of 104 new psychoactive substances (NPS) and other drugs of abuse in oral fluid by LC-MS-MS. J Anal Toxicol. 2020;44:697–707.
42. Ogunbodede O, McCombs D, Trout K, et al. New mescaline concentrations from 14 taxa/cultivars of *Echinopsis* spp. (Cactaceae) ("San Pedro") and their relevance to shamanic practice. J Ethnopharmacol. 2010;131:356–362.
43. Wyatt MF, Stein BK, Brenton AG. Characterization of various analytes using matrix-assisted laser desorption/ionization time-of-flight mass spectrometry and 2-[(2E)-3-(4-tert-butylphenyl)-2-methylprop-2-enylidene]malononitrile matrix. Anal Chem. 2006; 78:199–206.
44. Zhou L, Wang X, Liu W, et al. Rapid identification of the "smart drug" modafinil in suspicious tablets by DART-HRMS combined with micropunching. Anal Methods. 2020;12:1430–1440.
45. Yang S, Shi Y, Chen Z, et al. Detection of mescaline in human hair samples by UPLC-MS/MS: application to 19 authentic forensic cases. J Chromatogr B Analyt Technol Biomed Life Sci. 2022;1195:123202.
46. Vilhena NQ, Gil R, Llorca E, et al. Physico-chemical and microstructural changes during the drying of persimmon fruit cv. Rojo Brillante harvested in two maturity stages. Foods. 2020;9:870.
47. Schwartz SA, Reyzer ML, Caprioli RM. Direct tissue analysis using matrix-assisted laser desorption/ionization mass spectrometry: practical aspects of sample preparation. J Mass Spectrom. 2003;38:699–708.
48. Chaurand P, Norris JL, Cornett DS, et al. New developments in profiling and imaging of proteins from tissue sections by MALDI mass spectrometry. J Proteome Res. 2006;5:2889–2900.
49. Goodwin RJ, Pennington SR, Pitt AR. Protein and peptides in pictures: imaging with MALDI mass spectrometry. Proteomics. 2008;8:3785–3800.
50. Cazares LH, Troyer D, Mendrinos S, et al. Imaging mass spectrometry of a specific fragment of mitogen-activated protein kinase/extracellular signal-regulated kinase kinase kinase 2 discriminates cancer from uninvolved prostate tissue. Clin Cancer Res. 2009;15:5541–5551.
51. Kaspar S, Peukert M, Svatos A, et al. MALDI-imaging mass spectrometry - an emerging technique in plant biology. Proteomics. 2011;11:1840–1850.
52. Bøgeskov Schmidt F, Heskes AM, Thinagaran D, et al. Mass spectrometry based imaging of labile glucosides in plants. Front Plant Sci. 2018;9:892.
53. Walch A, Rauser S, Deininger SO, et al. MALDI imaging mass spectrometry for direct tissue analysis: a new frontier for molecular histology. Histochem Cell Biol. 2008;130:421–434.
54. Caldwell RL, Caprioli RM. Tissue profiling by mass spectrometry: a review of methodology and applications. Mol Cell Proteomics. 2005;4:394–401.
55. Lee H, Lai YH, Ou YM, et al. Enhancing carbohydrate ion yield by controlling crystalline structures in matrix-assisted laser desorption/ionization mass spectrometry. Anal Chim Acta. 2017;994: 49–55.
56. Ying Z, Haojie L. Enhanced ionization of phosphatidylcholines during MALDI mass spectrometry using DCTB as matrix. Chin Chem. 2012;30:2091–2096.
57. Li S, Zhang Y, Liu J, et al. Electrospray deposition device used to precisely control the matrix crystal to improve the performance of MALDI MSI. Sci Rep. 2016;6:37903.
58. Kaletaş BK, van der Wiel IM, Stauber J, et al. Sample preparation issues for tissue imaging by imaging MS. Proteomics. 2009;9: 2622–2633.
59. Xie H, Wu R, Hung YLW, et al. Development of a matrix sublimation device with controllable crystallization temperature for MALDI mass spectrometry imaging. Anal Chem. 2021;93:6342–6347.
60. Calvano CD, Monopoli A, Cataldi TRI, et al. MALDI matrices for low molecular weight compounds: an endless story? Anal Bioanal Chem. 2018;410:4015–4038.
61. Jovanović M, Peter-Katalinić J. Negative ion MALDI-TOF MS, ISD and PSD of neutral underivatized oligosaccharides without anionic dopant strategies, using 2,5-DHAP as a matrix. J Mass Spectrom. 2016;51:111–122.
62. Tsarbopoulos A, Karas M, Strupat K, et al. Comparative mapping of recombinant proteins and glycoproteins by plasma desorption and matrix-assisted laser desorption/ionization mass spectrometry. Anal Chem. 1994;66:2062–2070.
63. Leisner A, Rohlfing A, Berkenkamp S, et al. Infrared laser post-ionization of large biomolecules from an IR-MALD(I) plume. J am Soc Mass Spectrom. 2004;15:934–941.
64. Lin HY, Song BF, Ni CK. Fluorescence quantum yields of matrices used in ultraviolet matrix-assisted laser desorption/ionization. Rapid Commun Mass Spectrom. 2020;34:e8846.
65. Soltwisch J, Jaskolla TW, Dreisewerd K. Color matters—material ejection and ion yields in UV-MALDI mass spectrometry as a function of laser wavelength and laser fluence. J am Soc Mass Spectrom. 2013;24:1477–1488.
66. Aubriet F. Laser-induced Fourier transform ion cyclotron resonance mass spectrometry of organic and inorganic compounds: methodologies and applications. Anal Bioanal Chem. 2007;389: 1381–1396.
67. Lee C, Inutan ED, Chen JL, et al. Toward understanding the ionization mechanism of matrix-assisted ionization using mass spectrometry experiment and theory. Rapid Commun Mass Spectrom. 2021;35:e8382.
68. Pan M, Xiang P, Yu Z, et al. Development of a high-throughput screening analysis for 288 drugs and poisons in human blood using Orbitrap technology with gas chromatography-high resolution accurate mass spectrometry. J Chromatogr a. 2019;1587: 209–226.
69. Laurichesse M, Gicquel T, Moreau C, et al. Histamine quantification in human plasma using high resolution accurate mass LC-MS technology. Clin Biochem. 2016;49:111–116.
70. Yang H, Wang X, Liu M, et al. Detection of amfepramone and its metabolite cathinone in human hair: application to a uthentic cases of amfepramone use. Drug Test Anal. 2022;14: 101–109.
71. Ji JJ, Yan H, Xiang P, et al. An LC-MS/MS method for the simultaneous determination of 12 psychotropic drugs and metabolites in hair: identification of acute quetiapine poisoning using hair root. Forensic Sci Int. 2019;301:341–349.
72. Maurer HH. Current role of liquid chromatography–mass spectrometry in clinical and forensic toxicology. Anal Bioanal Chem. 2007;388:1315–1325.
73. Borroto Fernandez E, Peterseil V, Hackl G, et al. Distribution of chemical phenotypes (Chemotypes) in European agricultural hemp (*Cannabis sativa L.*). Cultivars J Forensic Sci. 2020;65:715–721.
74. Danziger N, Bernstein N. Shape matters: plant architecture affects chemical uniformity in large-size medical cannabis plants. Plants (Basel, Switzerland). 2021;10:1834.
75. De Backer B, Maebe K, Verstraete AG, et al. Evolution of the content of THC and other major cannabinoids in drug-type cannabis cuttings and seedlings during growth of plants. J Forensic Sci. 2012;57:918–922.

76. Safa N, Trobec T, Holland DC, et al. Spatial distribution and stability of cholinesterase inhibitory protoberberine alkaloids from Papaver setiferum. J Nat Prod. 2022;85:215–224.
77. Brito-da-Costa AM, Dias-da-Silva D, Gomes NGM, et al. Toxicokinetics and toxicodynamics of ayahuasca alkaloids *N,N*-dimethyltryptamine (DMT), harmine, harmaline and tetrahydroharmine: clinical and forensic impact. Pharmaceuticals (Basel, Switzerland). 2020;13:334.
78. Hamill J, Hallak J, Dursun SM, et al. Ayahuasca: psychological and physiologic effects, pharmacology and potential uses in addiction and mental illness. Curr Neuropharmacol. 2019;17:108–128.
79. Reti L, Castrillón JA. Cactus alkaloids I. *Trichocereus terscheckii* (Parmentier) britton and rose. J Am Chem Soc. 1951;73: 1767–1769.
80. Longo CM, Musah RA. An efficient ambient ionization mass spectrometric approach to detection and quantification of the mescaline content of commonly abused cacti from the *Echinopsis* genus. J Forensic Sci. 2020;65:61–66.
81. Klein MT, Kalam M, Trout K, et al. Mescaline concentrations in three principal tissues of *Lophophora williamsii* (Cactaceae): implications for sustainable harvesting practices. Haseltonia. 2015;20:34–42.
82. Halpern JH, Sherwood AR, Hudson JI, et al. Psychological and cognitive effects of long-term peyote use among native Americans. Biol Psychiatry. 2005;58:624–631.
83. Gambelunghe C, Marsili R, Aroni K, et al. GC-MS and GC-MS/MS in PCI mode determination of mescaline in peyote tea and in biological matrices. J Forensic Sci. 2013;58:270–278.